Baryonic acceleration closure across gas-rich dwarfs, disk galaxies, and galaxy clusters

Federico Quinteros[a,*]

[a]*Independent researcher, Montevideo, Uruguay*

Abstract

The radial acceleration relation connects the observed dynamical acceleration with the acceleration generated by observed baryons. In ordinary rotationally supported disks, this empirical relation is well described by a galactic acceleration scale of order $a_0 \simeq 1.2 \times 10^{-10}\,\mathrm{m\,s^{-2}}$, as in MOND/RAR phenomenology. Gas-rich dwarfs and galaxy clusters occupy different effective acceleration regimes because their baryons have different geometry, stability, pressure support, depletion, and confinement. This work formulates a common algebraic closure,

$$g_{\mathrm{pred}} = \frac{1}{2}\left[g_{\mathrm{bar}} + \sqrt{g_{\mathrm{bar}}^2 + 4g_{\mathrm{bar}}a_U}\right],$$

while allowing the effective scale a_U to be constructed from regime-specific baryonic physics. In LITTLE THINGS, the gas branch uses the effective gas-sheet field, Toomre participation, and an explicit asymmetric-drift pressure-support extension. In SPARC, a new structural branch is incorporated: a global scale $\widehat{a}_{U,d}$ is obtained from M_{HI}, R_d, and R_{HI}, without using g_{obs}, through the anchor $2G(1.33M_{\mathrm{HI}})/R_d^2$ and a geometric dilution factor for the H I extent. This branch recovers the scale of a_0 and strongly improves on the Newtonian baryonic model, although it does not yet outperform the fixed galactic RAR pointwise. In external CLASH regions, the intracluster branch follows from a depleted cosmic baryon fraction $f_{\mathrm{ICM}} = Y_{\mathrm{ICM}} f_{b,\mathrm{cos}}$, explaining a scale close to $2 \times 10^{-9}\,\mathrm{m\,s^{-2}}$ without fitting g_{tot}. In central CLASH regions, ACCEPT/CLASH hydrostatic support is combined with virial and triaxial geometric confinement. The result is not a covariant theory of gravity and is not presented as a replacement for dark matter. It is a falsifiable phenomenological closure of acceleration scales that organizes the hierarchy $10^{-11} \to 10^{-10} \to 10^{-9}\,\mathrm{m\,s^{-2}}$ through baryonic geometry, effective participation, and confinement.

Keywords: radial acceleration relation, disk galaxies, dwarf irregular galaxies, galaxy clusters, intracluster medium, gravitational lensing, MOND

1. Introduction

The empirical radial acceleration relation (RAR) links the total dynamical acceleration to the acceleration inferred from the observed baryonic mass distribution. In rotationally supported galaxies, the SPARC sample provides the reference data set, combining Spitzer photometry and rotation curves for 175 nearby disk galaxies [16]. In that regime, the relation is commonly expressed through a characteristic acceleration

$$a_0 \simeq 1.2 \times 10^{-10}\,\mathrm{m\,s^{-2}}, \tag{1}$$

which is the usual galactic scale in MOND and RAR phenomenology [18, 2, 17]. If the closure scale equals a_0, the low-acceleration limit becomes

$$g_{\mathrm{dyn}} \simeq \sqrt{g_{\mathrm{bar}}a_0}, \tag{2}$$

the familiar deep-MOND/RAR form. The present paper does not introduce a_0 as a new fitted parameter. It uses it as the historically established galactic scale, and then asks whether that scale and the scales of other regimes can be traced to independent baryonic and structural observables.

Extending the galactic RAR to gas-rich dwarfs and clusters is not automatic. Gas-rich dwarf irregulars are not simply cold low-mass disks. Their neutral gas can be partly pressure-supported, their velocity dispersion can be dynamically relevant, and asymmetric-drift corrections can substantially affect the inferred circular velocity [10, 11]. Galaxy clusters are still more different. Their dominant baryons are hot intracluster plasma, brightest-cluster-galaxy (BCG) stars, intracluster light (ICL), and satellite galaxies, all embedded in a three-dimensional and often triaxial potential. In CLASH, Tian et al. found a cluster RAR scale

$$g_{\ddagger} = (2.02 \pm 0.11) \times 10^{-9}\,\mathrm{m\,s^{-2}}, \tag{3}$$

well above the ordinary galactic value [22].

The aim of this work is deliberately limited. It does not propose a fundamental action and does not claim that dark matter is unnecessary. It proposes a scale-level closure: a common algebraic map between g_{bar} and g_{pred}, with the effective scale a_U computed differently in regimes with different baryonic geometry, stability, depletion, and confinement. The organizing

*Corresponding author.
Email address: federico.uy@vera.com.uy (Federico Quinteros)

question is whether the hierarchy

$$10^{-11}, \quad 10^{-10}, \quad 10^{-9}\ \mathrm{m\,s^{-2}} \tag{4}$$

can be traced to baryonic anchors and effective participation, rather than to disconnected numerical constants.

The paper is organized as follows. Section 2 derives the common closure and its inverse. Section 3 explains the baryonic anchors. Section 4 keeps the radial-shape constraint explicit. Sections 5, 6, 7, and 8 present the LITTLE THINGS, SPARC, external CLASH, and central CLASH branches. Section 9 compares the branch closure with fixed galactic RAR/MOND baselines. Section 10 states the limitations and falsifiable predictions.

2. Common algebraic closure and predictive participation

The common closure is

$$g_{\mathrm{pred}} = \frac{1}{2}\left[g_{\mathrm{bar}} + \sqrt{g_{\mathrm{bar}}^2 + 4g_{\mathrm{bar}}a_U}\right]. \tag{5}$$

It is the positive root of

$$g^2 - g_{\mathrm{bar}}g - g_{\mathrm{bar}}a_U = 0. \tag{6}$$

For $g_{\mathrm{bar}} \gg a_U$, Eq. (5) recovers $g_{\mathrm{pred}} \simeq g_{\mathrm{bar}}$. For $g_{\mathrm{bar}} \ll a_U$, it gives $g_{\mathrm{pred}} \simeq \sqrt{g_{\mathrm{bar}}a_U}$. Thus $a_U = a_0$ reproduces the ordinary deep galactic RAR limit, but the algebra does not require the same a_U in all systems.

If a measured dynamical field g_{dyn} is known, Eq. (6) can be inverted exactly:

$$a_{\mathrm{req}} = \frac{g_{\mathrm{dyn}}(g_{\mathrm{dyn}} - g_{\mathrm{bar}})}{g_{\mathrm{bar}}}. \tag{7}$$

With

$$\phi_{\mathrm{obs}} \equiv \frac{g_{\mathrm{bar}}}{g_{\mathrm{dyn}}}, \tag{8}$$

this becomes

$$a_{\mathrm{req}} = g_{\mathrm{bar}}\frac{1-\phi_{\mathrm{obs}}}{\phi_{\mathrm{obs}}^2}. \tag{9}$$

Equation (9) is algebraically exact, but it is diagnostic if ϕ_{obs} uses the final measured field. A branch becomes predictive only when a_U is obtained from independent baryonic, thermodynamic, geometric, or cosmological information.

The corresponding predictive participation is obtained directly from Eq. (5):

$$\widehat{\phi}_U(r) = \frac{g_{\mathrm{bar}}}{g_{\mathrm{pred}}} = \frac{2}{1+\sqrt{1+4\widehat{a}_U(r)/g_{\mathrm{bar}}(r)}}. \tag{10}$$

Thus the framework distinguishes two objects:

$$\phi_{\mathrm{obs}} = g_{\mathrm{bar}}/g_{\mathrm{dyn}}, \qquad \text{diagnostic}, \tag{11}$$

$$\widehat{\phi}_U = g_{\mathrm{bar}}/g_{\mathrm{pred}}, \qquad \text{predictive if } \widehat{a}_U \text{ is independent}. \tag{12}$$

This distinction is essential in SPARC and CLASH. It prevents the inverse identity from being mistaken for a prediction.

The programmatic statement is

$$a_U(r) \sim a^{\mathrm{geo}}_{\mathrm{bar,char}}(r)K_{\mathrm{eff}}(r), \tag{13}$$

where $a^{\mathrm{geo}}_{\mathrm{bar,char}}$ is the characteristic baryonic acceleration associated with the dominant geometry, and K_{eff} encodes participation, depletion, stability, thermodynamics, or confinement.

2.1. Relation to MOND interpolation functions

For fixed a_U, the closure can also be written in the usual MOND interpolation language. From Eq. (6),

$$g_{\mathrm{bar}} = \frac{g_{\mathrm{pred}}^2}{g_{\mathrm{pred}} + a_U}. \tag{14}$$

Defining

$$z = \frac{g_{\mathrm{pred}}}{a_U}, \tag{15}$$

Eq. (14) becomes

$$g_{\mathrm{bar}} = \mu(z)g_{\mathrm{pred}}, \qquad \mu(z) = \frac{z}{1+z}. \tag{16}$$

Equivalently, with

$$y = \frac{a_U}{g_{\mathrm{bar}}}, \tag{17}$$

Eq. (5) can be written as

$$g_{\mathrm{pred}} = \nu(y)g_{\mathrm{bar}}, \qquad \nu(y) = \frac{1}{2}\left(1+\sqrt{1+4y}\right). \tag{18}$$

Thus, for fixed a_U, the closure is equivalent to the simple MOND interpolation function. The novelty of the present work is not the interpolation function itself, but the construction of a_U from baryonic geometry, gas stability, cluster depletion, and hydrostatic–geometric confinement. When a_U varies with regime or radius, this equivalence should be read as a local effective interpolation, not as a covariant theory of gravity.

3. Baryonic acceleration anchors

Acceleration scales should not be introduced as isolated numbers when they can be traced to baryonic structure. For a sheet or flattened disk, the characteristic surface field is

$$a_{\mathrm{surf}} \sim 2\pi G\Sigma. \tag{19}$$

This is not a pointwise disk rotation law. It is a geometric acceleration scale: mass distributed over a surface produces a field proportional to the surface mass density, with $2\pi G$ as the natural sheet coefficient. In MOND-related work, the critical surface density is often written as $\Sigma_M = a_0/(2\pi G)$, so the connection between a_0 and surface density is not new [18, 17]. The present use is more specific: $2\pi G\Sigma$ is the baryonic-geometric anchor of the disk regime.

For representative disk surface densities

$$\Sigma_{\mathrm{bar}} \sim 50 - 100\ M_\odot\,\mathrm{pc}^{-2}, \tag{20}$$

one has $1\,M_\odot\,\mathrm{pc}^{-2} \simeq 2.09 \times 10^{-3}\,\mathrm{kg\,m}^{-2}$, and therefore

$$2\pi G\Sigma_{\mathrm{bar}} \sim (4.2 - 8.8) \times 10^{-11}\ \mathrm{m\,s}^{-2}. \tag{21}$$

This lies in the galactic $10^{-10}\,\mathrm{m\,s}^{-2}$ decade. The claim is not that $a_0 = 2\pi G\Sigma$ in every galaxy. The claim is that the order of magnitude of the galactic acceleration scale is naturally associated with observed baryonic surface densities in disks.

For clusters the relevant geometry changes. The baryonic anchor is not a sheet field but the enclosed baryonic field

$$a_{\mathrm{cl,char}}(r) = \frac{GM_{\mathrm{bar}}(< r)}{r^2}. \tag{22}$$

The distinction is geometrical. A disk is organized by surface density; a cluster is organized by enclosed mass in a hot three-dimensional potential. Applying the disk coefficient 2π to an arbitrary projected cluster surface density would mix incompatible geometries.

With the participation identity, a cluster with effective baryonic fraction $f_{\mathrm{bar,eff}}$ requires

$$a_{\mathrm{cl}} \sim g_{\mathrm{bar}} \frac{1 - f_{\mathrm{bar,eff}}}{f_{\mathrm{bar,eff}}^2}. \tag{23}$$

If $f_{\mathrm{bar,eff}} \simeq 1/8$, then $(1 - f)/f^2 = 56$. For $g_{\mathrm{bar}} \sim (2 - 5) \times 10^{-11}\,\mathrm{m\,s}^{-2}$, Eq. (23) gives $a_{\mathrm{cl}} \sim (1.1{-}2.8){\times}10^{-9}\,\mathrm{m\,s}^{-2}$, matching the cluster decade. The scale shift is therefore not merely numerical; it follows from geometry and low effective baryonic participation.

4. Radial shape of the curves

A useful acceleration closure must also preserve information about the radial shape of the curves. For a rotation curve,

$$V^2(R) = Rg_{\mathrm{dyn}}(R). \tag{24}$$

Taking logarithms and differentiating with respect to $\ln R$ gives

$$m(R) \equiv \frac{d\ln V}{d\ln R} = \frac{1}{2}\left[1 + \frac{d\ln g_{\mathrm{dyn}}}{d\ln R}\right]. \tag{25}$$

If $g_{\mathrm{dyn}} = g_{\mathrm{dyn}}(g_{\mathrm{bar}}, a_U)$, then

$$\frac{d\ln g_{\mathrm{dyn}}}{d\ln R} = \eta(R)s_{\mathrm{bar}}(R) + [1 - \eta(R)]s_U(R), \tag{26}$$

where

$$s_{\mathrm{bar}} = \frac{d\ln g_{\mathrm{bar}}}{d\ln R}, \qquad s_U = \frac{d\ln a_U}{d\ln R}, \tag{27}$$

and

$$\eta(R) = \frac{\partial\ln g_{\mathrm{dyn}}}{\partial\ln g_{\mathrm{bar}}}. \tag{28}$$

Therefore,

$$m(R) = \frac{1}{2}\left[1 + \eta s_{\mathrm{bar}} + (1 - \eta)s_U\right]. \tag{29}$$

Even if a_U is locally constant, the baryonic slope s_{bar} controls the rotation-curve shape. If a_U is radial, its slope s_U also contributes. This is why the framework treats geometry and radial baryonic structure as part of the closure, not merely as normalization factors.

5. Gas-rich dwarfs: LITTLE THINGS

The LITTLE THINGS survey provides high-resolution H I data for nearby dwarf galaxies [10]. Iorio et al. modeled the H I kinematics in three dimensions, providing circular velocities, gas velocity dispersions, surface densities, and asymmetric-drift corrected quantities [11]. Oh et al. provide complementary mass-model information for the same class of galaxies [20].

5.1. Gas-sheet and Toomre branch

The effective gas surface density is

$$\Sigma_{\mathrm{gas,eff}}(R) = 1.33\,\Sigma_{\mathrm{HI}}(R)(1 + f_{\mathrm{mol}}), \tag{30}$$

where 1.33 includes helium and $f_{\mathrm{mol}} = 0.23$ is the adopted correction for untraced or molecular gas, motivated by pressure and H I cloud studies in LITTLE THINGS. The bare gas-sheet field is

$$a_{\mathrm{gas},0}(R) = 2\pi G\Sigma_{\mathrm{gas,eff}}(R). \tag{31}$$

For representative effective gas surface densities of $5 - 20\,M_\odot\,\mathrm{pc}^{-2}$, this gives $(4.2 \times 10^{-12} - 1.8 \times 10^{-11})\,\mathrm{m\,s}^{-2}$, below the ordinary disk scale. A participation factor is therefore required.

The gas Toomre parameter is

$$Q_g(R) = \frac{\sigma_g(R)\kappa(R)}{\pi G\Sigma_{\mathrm{gas,eff}}(R)}, \tag{32}$$

where σ_g is the gas velocity dispersion and κ is the epicyclic frequency. We use the minimal participation prescription

$$\phi_Q(R) = \min\left(1, \frac{1}{Q_g(R)}\right). \tag{33}$$

The first-level gas branch is

$$a_g^{(Q)}(R) = 2\pi G\Sigma_{\mathrm{gas,eff}}(R)\left[1 + \frac{1 - \phi_Q(R)}{\phi_Q^2(R)}\right]. \tag{34}$$

The first term preserves the sheet field when the gas participates maximally. The second term is the algebraic participation amplification inherited from Eq. (9), with ϕ_Q replacing the diagnostic ϕ_{obs}.

For the present LITTLE THINGS consistency table, the branch gives

$$\mathrm{med}(a_g^{(Q)}) = 4.66 \times 10^{-11}\ \mathrm{m\,s}^{-2}, \tag{35}$$

with

$$\mathrm{med}(Q_g) = 3.31, \qquad \mathrm{med}(\phi_Q) = 0.302. \tag{36}$$

The median velocity-equivalent error of the Toomre-only branch is 0.149 pointwise and 0.137 by object in the original consistency table. This is not yet an optimal pointwise law for dwarf galaxies. Its role is to replace a bare numerical gas-branch scale by a physically interpretable scale built from $\Sigma_{\mathrm{gas,eff}}$, σ_g, κ, and Q_g.

Table 1: Physical interpretation of the acceleration hierarchy. Entries are scale-level statements, not complete radial laws in all regimes.

Regime	Baryonic anchor	Effective modifier	Scale
Gas-rich dwarfs	$2\pi G\Sigma_{\rm gas,eff}$	Toomre participation and gas pressure support	10^{-11}
Ordinary disks	$2G(1.33M_{\rm HI})/R_d^2$ and $2\pi G\Sigma_{\rm bar}$	H I geometric dilution, surface structure, and disk participation	10^{-10}
Clusters	$GM_{\rm bar}(<r)/r^2$	Depletion, low baryonic participation, hydrostatic and geometric confinement	10^{-9}

5.2. Pressure-support extension through asymmetric drift

The Toomre branch captures gas surface density and stability, but by itself it does not account for the pressure-support correction that converts the observed H I rotation field into circular support. In gas-rich dwarfs, the measured rotation velocity can be comparable to the gas velocity dispersion. The radial momentum equation gives

$$V_c^2(R) - V_{\rm rot}^2(R) = V_A^2(R), \tag{37}$$

where V_A is the asymmetric-drift correction. In the notation used by Iorio et al.,

$$V_A^2(R) = -R\sigma_{\rm HI}^2(R)\frac{d\ln[\rho_{\rm gas}(R)\sigma_{\rm HI}^2(R)]}{dR}. \tag{38}$$

For a thin H I layer with approximately constant thickness this becomes

$$V_A^2(R) = -\sigma_{\rm HI}^2(R)\frac{d\ln[\Sigma_{\rm HI}(R)\sigma_{\rm HI}^2(R)]}{d\ln R}. \tag{39}$$

The corresponding pressure-support acceleration is

$$g_{\rm AD}(R) = \frac{V_A^2(R)}{R}. \tag{40}$$

This is not a fitted multiplier. It follows from the radial momentum equation of the gas and is required whenever the validation target is the circular field rather than the raw gas rotation field.

The pressure–stability implementation is

$$g_{\rm pred}^{\rm dIrr}(R) = C[g_{\rm bar}(R), a_g^{(Q)}(R)] + g_{\rm AD}(R), \tag{41}$$

where

$$C[g_{\rm bar}, a] = \frac{1}{2}\left[g_{\rm bar} + \sqrt{g_{\rm bar}^2 + 4g_{\rm bar}a}\right]. \tag{42}$$

Equation (41) should not be applied by double-counting the same asymmetric-drift correction. Its interpretation is that the Toomre branch supplies the stability-controlled acceleration scale, while $g_{\rm AD}$ supplies the additional pressure-support acceleration needed to compare with the circular field.

Table 2 shows a systematic improvement over the Toomre-only branch in median error and in the fraction of points within fixed tolerance, although the RMS is still sensitive to outliers in the broader hybrid samples. The derived asymmetric-drift correction reproduces the tabulated correction with a median error of only a few km s^{-1}. Thus the dwarf branch is better described as a pressure–stability closure than as a pure Toomre branch. It is still not a final universal radial law for dwarf galaxies, because V_A is sensitive to profile smoothing, inclination, gas thickness, perturbations, and the consistency of the adopted baryonic mass model.

6. Disk galaxies: SPARC

The SPARC mass models provide R, $V_{\rm obs}$, $V_{\rm gas}$, $V_{\rm disk}$, $V_{\rm bul}$, surface-brightness profiles, disk scale lengths, H I masses, H I radii, and quality flags [16]. The dynamical and baryonic accelerations are

$$g_{\rm obs} = \frac{V_{\rm obs}^2}{R}, \qquad g_{\rm bar} = \frac{V_{\rm bar}^2}{R}, \tag{43}$$

with

$$V_{\rm bar}^2 = V_{\rm gas}|V_{\rm gas}| + 0.5V_{\rm disk}^2 + 0.7V_{\rm bul}^2. \tag{44}$$

The term $V_{\rm gas}|V_{\rm gas}|$ preserves the tabulated sign of the gas component. In the SPARC table, $V_{\rm gas}$ already includes the factor 1.33 for helium.

6.1. Direct discrepancy and inverse scale

The exact inverse scale is

$$a_{\rm diag}^{\rm SPARC} = g_{\rm bar}\frac{1-\phi_{\rm disk}}{\phi_{\rm disk}^2}, \qquad \phi_{\rm disk} = \frac{g_{\rm bar}}{g_{\rm obs}}. \tag{45}$$

This is diagnostic because it uses $g_{\rm obs}$.

The most conservative predictive quantity is the direct discrepancy

$$\Delta g \equiv g_{\rm obs} - g_{\rm bar}. \tag{46}$$

It is related to the inverse closure scale through

$$a_{\rm diag} = \frac{\Delta g}{\phi_{\rm disk}}. \tag{47}$$

Thus a prediction of Δg is not yet a complete pointwise prediction of a_U unless $\phi_{\rm disk}$ is predicted independently.

The photometric-surface estimator is

$$\Sigma_{\rm pred}(R) = \Upsilon_d S\, B_{\rm disk}(R) + \Upsilon_b S\, B_{\rm bul}(R) + \frac{1.33M_{\rm HI}}{\pi R_{\rm HI}^2}, \tag{48}$$

Table 2: LITTLE THINGS pressure-support audit. The metric is the median velocity-equivalent error unless otherwise stated. The derived V_A is computed from the H I pressure-gradient relation in Eq. (39).

Audit sample	Points / galaxies	Q only	$Q + V_A^2/R$ tabulated	$Q + V_A^2/R$ derived	median $\lvert V_A^{\rm der} - V_A^{\rm tab}\rvert$
clean radial QC	125 / 9	0.161	0.149	0.148	2.53 km s^{-1}
clean linc0/bdist0	145 / 10	0.183	0.170	0.166	2.61 km s^{-1}
hybrid model	219 / 16	0.204	0.193	0.186	3.15 km s^{-1}
hybrid data	214 / 16	0.218	0.203	0.201	3.26 km s^{-1}

with $\Upsilon_d = 0.5$ and $\Upsilon_b = 0.7$. The gas term is a global H I surface-density contribution, not a detailed radial H I reconstruction. The exponential-disk geometry factor is

$$F_{\rm exp}(x) = e^x y\,[I_0(y)K_0(y) - I_1(y)K_1(y)], \tag{49}$$

$$x = R/R_d, \qquad y = x/2. \tag{50}$$

The predictive discrepancy branch is

$$\widehat{\Delta g}_d(R) = 2\pi G\Sigma_{\rm pred}(R)F_{\rm exp}(R/R_d). \tag{51}$$

For the cut $Q_{\rm SPARC} \le 2$, $T_{\rm SPARC} \le 8$, and $0.5R_d \le R \le 4R_d$, the audit retains 102 galaxies and 1414 radial points. It gives

$$\mathrm{med}(g_{\rm obs} - g_{\rm bar}) = 5.28 \times 10^{-11}\ \mathrm{m\,s^{-2}}, \tag{52}$$

and

$$\mathrm{med}(\widehat{\Delta g}_d) = 5.31 \times 10^{-11}\ \mathrm{m\,s^{-2}}. \tag{53}$$

In the same cut, the inverse diagnostic scale is

$$\mathrm{med}(a_{\rm diag}^{\rm SPARC}) = 1.18 \times 10^{-10}\ \mathrm{m\,s^{-2}}, \tag{54}$$

because $a_{\rm diag} = \Delta g/\phi_{\rm disk}$. This first branch shows that the disk surface structure predicts the direct discrepancy, but it does not by itself close the pointwise participation.

6.2. Structural H I scale for a_U and predictive participation

To close the SPARC branch at scale level, a global structural scale is introduced using only $M_{\rm HI}$, R_d, and $R_{\rm HI}$. The starting point is the global gas surface-field anchor. If the gas mass is evaluated on the stellar scale R_d, then

$$\Sigma_{{\rm gas},d} \sim \frac{M_{\rm gas}}{\pi R_d^2}, \tag{55}$$

and the associated surface field is

$$a_{\rm base} = 2\pi G\frac{M_{\rm gas}}{\pi R_d^2} = \frac{2GM_{\rm gas}}{R_d^2}. \tag{56}$$

With $M_{\rm gas} = 1.33M_{\rm HI}$,

$$a_{\rm base} = \frac{2G(1.33M_{\rm HI})}{R_d^2}. \tag{57}$$

Equation (57) is a global scale, not a radial law. It must be corrected for the fact that the H I disk usually extends well beyond the stellar disk. Define

$$\chi_{\rm HI} = \frac{R_{\rm HI}}{R_d}, \qquad \chi_0 = \mathrm{median}(R_{\rm HI}/R_d) = 5.567. \tag{58}$$

The value χ_0 is not fitted to velocities or to a_0; it is the observed median H I relative extent in SPARC.

The effective participation of the gas should decrease when $R_{\rm HI}/R_d$ increases. A radial dilution gives exponent $p = 1$, while an ideal sheet-like surface dilution gives $p = 2$. Since real H I has finite thickness, velocity dispersion, turbulence, and coupling to the stellar potential, we consider the geometric family

$$K_{\rm HI}(p) = \left(\frac{\chi_0}{\chi_{\rm HI}}\right)^p, \qquad 1 \le p \le 2. \tag{59}$$

The case $p = 3/2$ is adopted as the fiducial central value between the radial and surface limits; it is not asserted as a first-principles derivation. The structural scale is

$$\widehat{a}_{U,d}(p) = \frac{2G(1.33M_{\rm HI})}{R_d^2}\left(\frac{\chi_0}{R_{\rm HI}/R_d}\right)^p. \tag{60}$$

The fiducial case is

$$\widehat{a}_{U,d} = \frac{2G(1.33M_{\rm HI})}{R_d^2}\left(\frac{\chi_0}{R_{\rm HI}/R_d}\right)^{3/2}. \tag{61}$$

The orientation of the ratio in Eqs. (59)–(61) is physical: if the H I is more extended than typical, $R_{\rm HI}/R_d > \chi_0$, the effective participation decreases.

With this scale one obtains a predictive participation,

$$\widehat{\phi}_d(R) = \frac{2}{1 + \sqrt{1 + 4\widehat{a}_{U,d}/g_{\rm bar}(R)}} \tag{62}$$

and

$$g_{\rm pred}(R) = \frac{g_{\rm bar}(R)}{\widehat{\phi}_d(R)}. \tag{63}$$

This construction no longer uses $g_{\rm obs}$ to define the disk participation.

Table 3 shows that scale recovery is not finely dependent on $p = 3/2$: the entire physical interval $1 \le p \le 2$ produces a scale of order $10^{-10}\,\mathrm{m\,s^{-2}}$. The fiducial case gives

$$\mathrm{med}(\widehat{a}_{U,d}) = 1.32 \times 10^{-10}\ \mathrm{m\,s^{-2}}, \tag{64}$$

close to the usual value $a_0 \simeq 1.2\times10^{-10}\,\mathrm{m\,s^{-2}}$, without inserting a_0 as an input.

The correct reading is therefore twofold. First, the galactic scale can be recovered from H I and photometric structure:

$$a_0 \sim \frac{2G(1.33M_{\rm HI})}{R_d^2}\left(\frac{\chi_0}{R_{\rm HI}/R_d}\right)^p, \qquad 1 \le p \le 2. \tag{65}$$

Table 3: Robustness test of the structural SPARC scale over the 171 galaxies with $R_{\rm HI} > 0$. The dispersion is $\sigma[\log_{10}(\widehat{a}_{U,d})]$. The kinematic metric uses $\epsilon_V = |\sqrt{g_{\rm pred}/g_{\rm obs}} - 1|$.

p	med$(\widehat{a}_{U,d})$ [m s^{-2}]	$\sigma \log \widehat{a}_U$	med$\lvert\epsilon_V\rvert$	RMS ΔV [km s^{-1}]	within 20%
1	1.23×10^{-10}	0.221	0.130	27.10	0.688
3/2	1.32×10^{-10}	0.152	0.119	25.95	0.711
2	1.37×10^{-10}	0.143	0.117	26.18	0.700

Table 4: Global SPARC comparison for the 171 galaxies with $R_{\rm HI} > 0$. The structural branch clearly improves on the Newtonian baryonic model, but the fixed RAR/MOND remains more accurate pointwise.

Model	med$\lvert\epsilon_V\rvert$	RMS ΔV
Baryonic Newtonian	0.402	58.62
fixed RAR/MOND a_0	0.105	22.90
SPARC structural $p = 3/2$	0.119	25.95

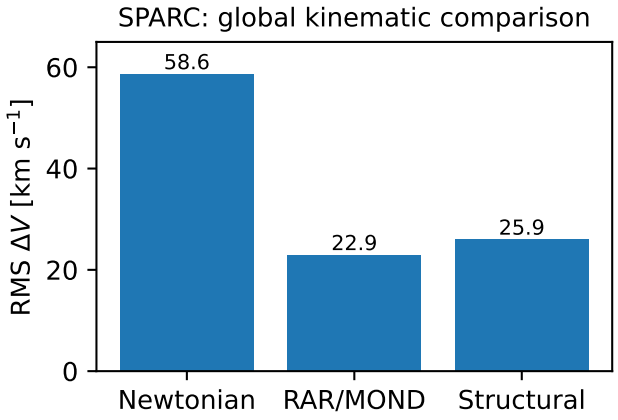

Figure 1: Global kinematic comparison in SPARC. The structural H I scale recovers a_0 and strongly improves over the Newtonian model, but it does not yet outperform the fixed RAR/MOND inside SPARC.

Second, this global scale is not yet a final radial law. The fixed galactic RAR retains a pointwise advantage. A more local version should replace global $M_{\rm HI}$ and $R_{\rm HI}$ with profiles $\Sigma_{\rm HI}(R)$, gas thickness, velocity dispersion, stability, and radial gas fraction.

7. External CLASH branch: depleted ICM fraction

For the CLASH RAR table of Tian et al. [22], the diagnostic baryon fraction is

$$f_{\rm bar}^{\rm diag} = \frac{g_{\rm bar}}{g_{\rm tot}}, \tag{66}$$

which gives

$$a_{\rm ICM}^{\rm diag} = g_{\rm bar} \frac{1 - f_{\rm bar}^{\rm diag}}{(f_{\rm bar}^{\rm diag})^2}. \tag{67}$$

Over the 84 CLASH points,

$$\mathrm{med}(f_{\rm bar}^{\rm diag}) = 0.127, \qquad \mathrm{med}(a_{\rm ICM}^{\rm diag}) = 1.89{\times}10^{-9}\ \mathrm{m\,s^{-2}}. \tag{68}$$

Table 5: Propagation of cluster baryon depletion. We take $f_{b,\cos} = 0.156$.

$Y_{\rm ICM}$	$\widehat{f}_{\rm ICM}$	$K_{\rm ICM}$
0.75	0.117	64.5
0.80	0.1248	56.2
0.85	0.133	49.2

For $R \geq 100$ kpc,

$$\mathrm{med}(f_{\rm bar}^{\rm diag}) = 0.115, \qquad \mathrm{med}(a_{\rm ICM}^{\rm diag}) = 1.99{\times}10^{-9}\ \mathrm{m\,s^{-2}}. \tag{69}$$

These values show why the cluster scale lies in the 10^{-9} m s^{-2} decade.

To make the external branch predictive at scale level, the diagnostic fraction is replaced by a depleted cosmic baryon fraction:

$$\widehat{f}_{\rm ICM} = Y_{\rm ICM} f_{b,\cos}. \tag{70}$$

The factor

$$f_{b,\cos} = \frac{\Omega_b}{\Omega_m} \simeq 0.156 \tag{71}$$

comes from CMB cosmology, not from fitting CLASH [21]. The factor $Y_{\rm ICM}$ represents baryonic depletion of clusters within the evaluation radius; the literature on gas fractions, X-rays, SZ measurements, and simulations uses precisely depletion factors relative to the cosmic fraction, with typical scale-level values $Y_{\rm ICM} \sim 0.75 - 0.85$ for massive clusters within radii such as R_{500} [12, 19, 8]. We adopt the fiducial value

$$Y_{\rm ICM} = 0.80, \tag{72}$$

which gives

$$\widehat{f}_{\rm ICM} = 0.80 \times 0.156 = 0.1248, \tag{73}$$

and

$$K_{\rm ICM} = \frac{1 - \widehat{f}_{\rm ICM}}{\widehat{f}_{\rm ICM}^2} = 56.19. \tag{74}$$

The external ICM branch is

$$\widehat{a}_{\rm ICM}(R) = K_{\rm ICM} g_{\rm bar}(R), \qquad R \geq 100\ \mathrm{kpc}. \tag{75}$$

It does not use $g_{\rm tot}$ as an input. On the 84-point CLASH table it gives a by-object median velocity-equivalent error of 0.134 and $\mathrm{med}(g_{\rm pred}/g_{\rm tot}) = 1.019$. For $R \geq 100$ kpc, it gives error 0.116 and $\mathrm{med}(g_{\rm pred}/g_{\rm tot}) = 0.922$.

Propagation of the depletion range shows the robustness of the scale. For $Y_{\rm ICM} = 0.75 - 0.85$,

$$\widehat{f}_{\rm ICM} = 0.117 - 0.133, \tag{76}$$

and

$$K_{\rm ICM} = 49 - 65. \tag{77}$$

The lower effective depletion extreme gives the lower amplification, and vice versa. With typical external baryonic cluster fields

$$g_{\rm bar,cl} \sim (3.5 - 4.0) \times 10^{-11}\ {\rm m\,s^{-2}}, \tag{78}$$

the fiducial value gives

$$a_{\rm ICM} \sim 56.19(3.5 - 4.0) \times 10^{-11} = (1.97 - 2.25) \times 10^{-9}\ {\rm m\,s^{-2}}, \tag{79}$$

which falls on the scale $g_\ddagger \simeq 2{\times}10^{-9}\ {\rm m\,s^{-2}}$ reported in CLASH. Thus the cluster scale is obtained as a spherical baryonic field multiplied by low effective baryonic participation, not as an independent constant.

The next step is to replace the constant $Y_{\rm ICM}$ by a radial depletion law $Y_{\rm ICM}(r)$ constrained by X-ray, SZ, and gas-fraction measurements.

8. Central CLASH branch: ACCEPT and geometry

The central CLASH point is not an isolated SPARC-like galaxy. It is a BCG/ICL stellar component embedded in a cluster potential. If the BCG were treated as a locally baryon-dominated galaxy, the participation amplification would be artificially suppressed, while the lensing field remains cluster-dominated. The central branch must therefore combine local gas support with the cluster confinement field.

The hydrostatic acceleration associated with thermal pressure support is

$$g_{\rm HSE}(r) = \left|\frac{d\ln P_{\rm th}}{d\ln r}\right| \frac{k_B T(r)}{\mu m_p r}. \tag{80}$$

This is the scalar radial reduction of $\nabla P = -\rho_g \nabla\Phi$. In a triaxial cluster, the scalar spherical expression loses information about the geometry of $\nabla\Phi$. The central scale is therefore written as

$$a_{\rm core}(r) = \sqrt{g_{\rm HSE}(r)|\nabla\Phi_{\rm ell}(r)|}, \qquad r < 100\ {\rm kpc}. \tag{81}$$

Equivalently,

$$a_{\rm core}(r) = \sqrt{g_{\rm HSE}(r) G_{\rm geo}(r) \frac{GM_{500}}{2R_{500} r}}, \tag{82}$$

where

$$G_{\rm geo}(r) = \frac{|\nabla\Phi_{\rm ell}(r; M_{500}, c_{500}, q_a, q_b, \theta, \varphi)|}{GM_{500}/(2R_{500}r)}. \tag{83}$$

Thus $G_{\rm geo}$ is a ratio of fields, not a fitted normalization.

ACCEPT provides Chandra thermodynamic profiles, including pressure and temperature, for many clusters [4]. The central CLASH test has ACCEPT matches for 15 of the 20 central points; missing or invalid bins are replaced by physical MCXC/gNFW estimates rather than by residual information from the observed CLASH accelerations. With $G_{\rm geo} = 1$, the hydrostatic-virial branch already gives median central scales of 2.15×10^{-9}, 1.82×10^{-9}, and $1.53 \times 10^{-9}\ {\rm m\,s^{-2}}$ for the Tian/gNFW, MCXC/gNFW, and ACCEPT variants, respectively.

Table 6: Improvement of the central CLASH core when the published triaxial/line-of-sight geometry is used as $G_{\rm geo}$. The metric is the median of $|\sqrt{g_{\rm pred}/g_{\rm tot}} - 1|$ by object for the 20 central points.

Central baseline	$G_{\rm geo} = 1$	$G_{\rm geo} = f_{\rm geo}$
Tian/gNFW	0.118	0.106
MCXC/gNFW	0.129	0.113
ACCEPT/local	0.133	0.112

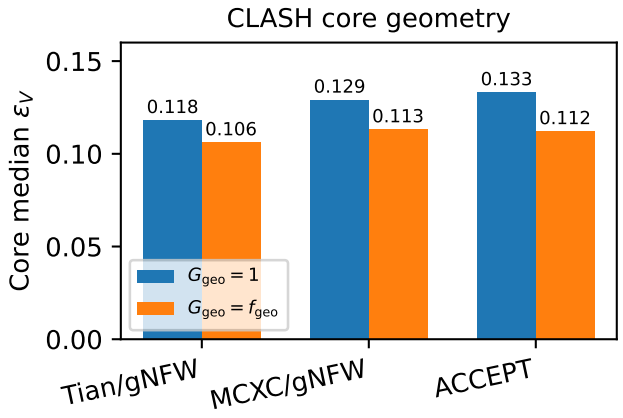

Figure 2: Effect of published CLASH line-of-sight/triaxial geometry on the central hydrostatic-virial branch. The improvement is consistent, but it is not yet a complete cluster-by-cluster radial prediction.

Published CLASH geometry permits a first no-fit correction. Umetsu et al. measure projected eNFW axis ratios and mass morphology for CLASH [24]. Chiu et al. perform a triaxial CLUMP-3D analysis with NFW axes, orientation, and mass-concentration constraints [5]. We use the literature line-of-sight/triaxial factor

$$f_{\rm geo} = \frac{L_\parallel}{\xi_s \sqrt{q_\perp}} \tag{84}$$

and take, in the first implementation,

$$G_{\rm geo}^{(0)} = f_{\rm geo}. \tag{85}$$

When individual posteriors are not used, the Chiu et al. B15-prior scaling gives

$$f_{\rm geo} \simeq 0.96 \left(\frac{M_{200}}{10^{15} M_\odot}\right)^{-0.21}. \tag{86}$$

This factor is not fitted to the residuals of the present closure.

The improvement in Table 6 is modest but systematic, and is obtained without fitting a new exponent or normalization. The logarithmic correlation between the published $G_{\rm geo}$ and the required $G_{\rm geo}$ is positive but weak: 0.17, 0.27, and 0.19 for the Tian/gNFW, MCXC/gNFW, and ACCEPT variants. A purely projected factor $(q_\perp + 1/q_\perp)/2$ does not robustly improve the core and is not used as the principal branch. The relevant piece is not sky-plane ellipticity alone; it is line-of-sight/triaxial confinement of the cluster potential.

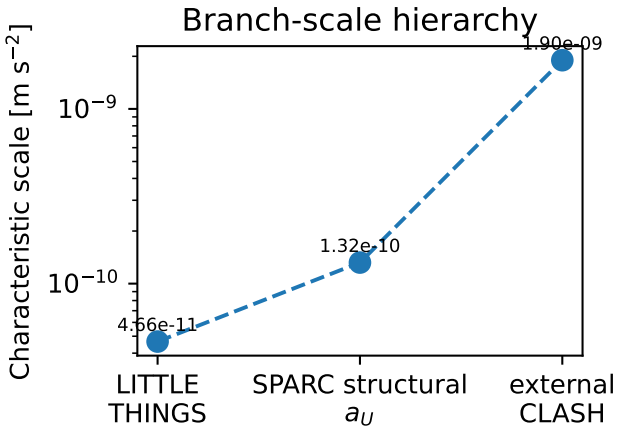

Figure 3: Characteristic scales by branch. The hierarchy follows baryonic geometry multiplied by participation or confinement: gas-rich dwarfs near 10^{-11}, ordinary disks near 10^{-10}, and clusters near 10^{-9} m s^{-2}.

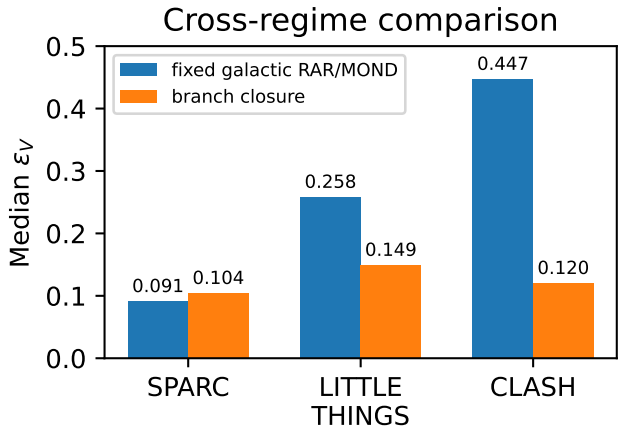

Figure 4: Fixed galactic RAR/MOND-like closure compared with the branch closure. The branch closure is not intended to outperform the SPARC-calibrated RAR inside SPARC alone; its advantage is cross-regime organization.

9. Comparison with fixed galactic RAR/MOND baselines

The velocity-equivalent error metric is

$$\epsilon_V = \left| \sqrt{g_{\rm pred}/g_{\rm obs}} - 1 \right|, \tag{87}$$

with $g_{\rm obs}$ replaced by $g_{\rm tot}$ for CLASH. The comparison in Table 7 is cross-regime. It does not claim that the structural SPARC branch outperforms the SPARC-calibrated RAR within SPARC, where the galactic RAR is already optimized.

In SPARC, the fixed galactic RAR remains a strong pointwise phenomenology. The present SPARC branch has a different role: it recovers the scale value of a_0 from independent H I structure and provides a predictive participation, although it does not yet outperform the fixed RAR pointwise. In LITTLE THINGS, the Toomre branch improves over an extrapolation of the fixed galactic scale; adding the asymmetric-drift pressure term further improves the clean dwarf audit from 0.161 to 0.148, although this is still not the final optimal dwarf-galaxy law. In CLASH, the fixed galactic scale fails by the construction of the regime itself: the cluster scale is set by depleted baryon fraction and hydrostatic-geometric confinement.

10. Interpretation, limitations, and falsifiable predictions

The scale branches can be summarized as

$$10^{-11}: \quad g_{\rm pred}^{\rm dIrr} = C[g_{\rm bar}, a_g^{(Q)}] + V_A^2/R, \tag{88}$$

$$10^{-10}: \quad \widehat{a}_{U,d}(p) = \frac{2G(1.33M_{\rm HI})}{R_d^2}\left(\frac{\chi_0}{R_{\rm HI}/R_d}\right)^p, \quad 1 \le p \le 2, \tag{89}$$

$$10^{-9}: \quad \widehat{a}_{\rm ICM} = g_{\rm bar}\frac{1-\widehat{f}_{\rm ICM}}{\widehat{f}_{\rm ICM}^2}, \tag{90}$$

$$\text{core}: \quad a_{\rm core} = \sqrt{g_{\rm HSE} G_{\rm geo} \frac{GM_{500}}{2R_{500}r}}. \tag{91}$$

The common principle is not a universal acceleration constant. It is a mapping from baryonic geometry to effective dynamical participation or confinement.

The framework has clear limitations. First, the LITTLE THINGS branch now includes an explicit asymmetric-drift pressure-support term and improves over the Toomre-only implementation, but it still requires larger homogeneous dwarf samples and sensitivity tests in $f_{\rm mol}$, Q_g, profile smoothing, gas thickness, inclination, the leading unity in Eq. (34), and possible double-counting of V_A. Second, the structural SPARC branch recovers the galactic scale and defines $\widehat{\phi}_d$ without using $g_{\rm obs}$, but it uses global $M_{\rm HI}$ and $R_{\rm HI}$; therefore, it is not yet a local radial law competitive with the fixed galactic RAR. A local version should replace the global mass by $\Sigma_{\rm HI}(R)$, gas thickness, turbulence, stability, and radial gas fraction. Third, the external CLASH branch uses a fiducial $Y_{\rm ICM}$ within an observed depletion range; a radial depletion law $Y_{\rm ICM}(r)$ must be independently constrained. Fourth, the central CLASH branch incorporates geometry, but $G_{\rm geo} = f_{\rm geo}$ remains a scale-level representation. The fully predictive calculation requires

$$G_{\rm geo}(r) = \frac{|\nabla\Phi_{\rm tri}(r; M_{500}, c_{500}, q_a, q_b, \theta, \varphi)|}{GM_{500}/(2R_{500}r)} \tag{92}$$

computed from individual triaxial posteriors.

These limitations make the framework falsifiable. If the pressure–stability dwarf branch fails in a larger homogeneous sample, the gas-participation and pressure-support hypothesis fails. If a local version of the SPARC scale does not improve pointwise residuals without inserting $g_{\rm obs}$, the disk branch remains a scale explanation and not a final radial law. If $Y_{\rm ICM}(r)$ or $|\nabla\Phi_{\rm tri}|$ do not reduce CLASH residuals without a new normalization, the cluster branch fails.

Table 7: Median velocity-equivalent errors. The fixed galactic RAR/MOND baseline is strong in SPARC but fragile if applied unchanged to gas-rich dwarfs and clusters. The branch closure improves cross-regime behavior while retaining explicit limitations.

Regime	Points	fixed galactic RAR/MOND	branch closure
SPARC disks, clean cut	1407	0.091	0.104
LITTLE THINGS	94 / 125	0.258	0.149 / 0.148
external plus central CLASH	84	0.447	0.106–0.134

11. Conclusions

This paper reformulates the multi-regime RAR problem as a baryonic closure of acceleration scales. The common algebraic map is simple, but the effective scale a_U is constructed from the dominant baryonic geometry and participation physics of each regime. The gas-rich dwarf branch uses gas surface density, Toomre participation, and asymmetric-drift pressure support. The SPARC branch now incorporates an H I structural scale that recovers the value of a_0 from $M_{\rm HI}$, R_d, and $R_{\rm HI}$, and defines a predictive participation without using $g_{\rm obs}$, although it does not yet outperform the fixed galactic RAR pointwise. The external CLASH branch follows from a depleted cosmic baryon fraction and explains why the cluster scale falls near $2\times10^{-9}\,\mathrm{m\,s^{-2}}$. The central CLASH branch combines hydrostatic support with virial and triaxial geometric confinement.

The result is not a final fundamental theory and is not a fully predictive radial law in every regime. It is a more constrained phenomenological framework in which the hierarchy

$$10^{-11} \rightarrow 10^{-10} \rightarrow 10^{-9}\,\mathrm{m\,s^{-2}} \tag{93}$$

is organized through baryonic geometry, depletion, stability, and confinement, rather than through unrelated constants.

Data and documentation availability

This work uses public observational data products and published documentation. No proprietary survey data are used.

The SPARC calculations use the SPARC sample table of Lelli, McGaugh and Schombert; the SPARC mass-model table `MassModels_Lelli2016c`; the tabulated radii, observed rotation velocities, gas velocity contribution, stellar-disk contribution, bulge contribution, disk scale lengths, H I masses and H I radii; and the SPARC rotation-curve/mass-model documentation associated with the public release.

The gas-rich dwarf-galaxy calculations use LITTLE THINGS survey documentation and galaxy-property tables from Hunter et al.; the Iorio et al. tilted-ring and asymmetric-drift-corrected kinematic profiles; the Iorio online `finalrot` tables, including radius, raw rotation velocity, asymmetric-drift correction, circular velocity, H I velocity dispersion and H I surface density; the Oh et al. LITTLE THINGS high-resolution mass-model and galaxy-property tables in VizieR `J/AJ/149/180`; the Hunter et al. LITTLE THINGS VizieR tables in `J/AJ/144/134`, used for global structural quantities such as optical scale lengths and H I content; and ROTMOD-style public rotation/mass-model components where the required baryonic terms are explicit.

The CLASH and cluster calculations use the Tian et al. CLASH radial-acceleration-relation data in VizieR `J/ApJ/896/70`, especially the machine-readable `fig2` table; the Tian et al. CLASH/BCG table in VizieR `J/ApJ/896/70/table1`; the published CLASH lensing and baryonic-mass information used to define total and baryonic radial accelerations; ACCEPT thermodynamic profiles from Cavagnolo et al., used as public X-ray thermodynamic context; published CLASH morphology, X-ray/lensing and triaxial-geometry constraints from the CLASH literature; Corasaniti et al. cluster gas-fraction and mass tables in VizieR `J/ApJ/911/82`, used for external cluster-regime stress tests involving `M500c` and `fgas`; and the public CLASH missing-mass/lensing reproduction files present in the local validation package, including the CLASH mass-profile tables and `fgasMACS` support table, used only where the required quantities are explicit.

The local-volume and auxiliary galaxy checks use the Updated Nearby Galaxy Catalog of Karachentsev et al. in VizieR `J/AJ/145/101`; Chandra normal-galaxy catalogue material from Kim et al. and other follow-up catalogues only as exclusion/context checks, not as resolved dynamical validation data.

The derived tables and scripts used to reproduce the numerical summaries are available from the author upon reasonable request.

Acknowledgements

The author thanks the public SPARC, LITTLE THINGS, ACCEPT, and CLASH teams for making their data products available to the community.

References

[1] M. Arnaud, G. W. Pratt, R. Piffaretti, H. Böhringer, J. H. Croston, E. Pointecouteau, A&A **517**, A92 (2010)

[2] J. Bekenstein, M. Milgrom, ApJ **286**, 7 (1984)

[3] M. Bonamigo, G. Despali, M. Limousin et al., MNRAS **449**, 3171 (2015)

[4] K. W. Cavagnolo, M. Donahue, G. M. Voit, M. Sun, ApJS **182**, 12 (2009)

[5] I.-N. Chiu, K. Umetsu, M. Sereno et al., ApJ **860**, 126 (2018)

[6] M. Donahue, G. M. Voit, A. Hoffer et al., ApJ **794**, 136 (2014)

[7] M. Donahue, T. Connor, K. Fogarty et al., ApJ **819**, 36 (2016)

[8] D. Eckert, S. Ettori, A. Pointecouteau et al., A&A **621**, A40 (2019)

[9] F. Feroz, M. P. Hobson, MNRAS **420**, 596 (2012)

[10] D. A. Hunter, D. Ficut-Vicas, T. Ashley et al., AJ **144**, 134 (2012)

[11] G. Iorio, F. Fraternali, C. Nipoti et al., MNRAS **466**, 4159 (2017)

[12] A. V. Kravtsov, D. Nagai, A. A. Vikhlinin, ApJ **625**, 588 (2005)

[13] P. S. Corasaniti, M. Sereno, S. Ettori, ApJ **911**, 82 (2021)

[14] I. D. Karachentsev, D. I. Makarov, E. I. Kaisina, AJ **145**, 101 (2013)

[15] D.-W. Kim, A. Cassity, B. Bhatt et al., ApJS **268**, 17 (2023)

[16] F. Lelli, S. S. McGaugh, J. M. Schombert, AJ **152**, 157 (2016)

[17] S. S. McGaugh, F. Lelli, J. M. Schombert, Phys. Rev. Lett. **117**, 201101 (2016)

[18] M. Milgrom, ApJ **270**, 365 (1983)

[19] D. Nagai, A. V. Kravtsov, A. Vikhlinin, ApJ **668**, 1 (2007)

[20] S.-H. Oh, D. A. Hunter, E. Brinks et al., AJ **149**, 180 (2015)

[21] Planck Collaboration, N. Aghanim et al., A&A **641**, A6 (2020)

[22] Y. Tian, K. Umetsu, C.-M. Ko, M. Donahue, I.-N. Chiu, ApJ **896**, 70 (2020)

[23] K. Umetsu, A. Zitrin, D. Gruen et al., ApJ **821**, 116 (2016)

[24] K. Umetsu, M. Sereno, M. Lieu et al., ApJ **860**, 104 (2018)